LITHOS 406–407 (2021) 106520

Contents lists available at ScienceDirect

LITHOS

journal homepage: www.elsevier.com/locate/lithos

Research Article

Bitu ophiolite in eastern Tibet: The last piece of the jigsaw puzzle in the Paleotethyan regime along the eastern Cimmerian continental margin

Shifeng Wang [a,*], Xiugen Fu [b], Yiduo Liu [c], Suoya Fan [c], Jian Wang [b], Zhonghai Wu [a]

[a] Institute of Geomechanics, Chinese Academy of Geological Sciences, Beijing 100081, China
[b] School of Geoscience and Technology, Southwest Petroleum University, Chengdu 610050, China
[c] Department of Earth and Atmospheric Sciences, University of Houston, TX 77204, USA

ARTICLE INFO

Keywords:
Paleotethyan Ocean
Bitu suture
Ophiolites
Zircon U—Pb ages
Geochemistry
Tibetan Plateau

ABSTRACT

As part of the eastern Cimmerian continent, the Qiangtang terrane played an important role in the evolution of the Pangea supercontinent. Recent studies suggest the Qiangtang terrane be divided into two parts along the Longmu Co-Shuanghu Paleotethyan suture, which connected with the Changning-Menglian suture as the boundary of the Cimmerian continents from the Laurasia. However, this proposal has been challenged by the absence of ophiolite mélanges in 700-km length in eastern Tibet. To fill this gap, here we investigate an ophiolite mélange suite, named Bitu, in eastern Tibet. The mélange includes blocks of serpentinites, gabbros, basalts, and minor radiolarian-bearing cherts. Zircon U—Pb dating indicates that the gabbro crystallized at ~265 Ma and one basalt sample has zircon ages that cluster at ~426 Ma. Geochemical analysis shows that the mafic rocks have oceanic island basalt (OIB) or mid-ocean ridge basalt (MORB) characteristics. This indicates an expanded ocean from the Late Silurian to the Middle Triassic in eastern Tibet, comparable to that of other Paleotethyan sutures. Thus, based on regional comparison, we infer that the Longmu Co-Shuanghu, Bitu, and Changning-Menglian sutures represent the vanished Paleotethyan Ocean that spanned over ~4000 km between the eastern Cimmerian and the Laurasia continents. Reconstruction of the Paleozoic plate tectonics provides robust evidence for terrane correlation from Pamir to Southeast Asia. Moreover, the pre-Cenozoic plate configuration proposed by this study questions the suggestions of 400–500 km offset in the Cenozoic along the Karakorum-Jiali-Ailaoshan fault system based on the correlation of the Rushan-Pshart with the Bangong-Nujiang suture and the correlation of the Jinshajiang with the Dien Bien Phu suture.

1. Introduction

The Pangea supercontinent was born by a series of sequentially amalgamated large continental masses, as well as arcs, back-arc basins, and micro-continents from the Cambrian to the Permian, such as the Siberia and North China/Tarim cratons that originated from the Laurasia continent, and the Cimmerian ribbon-like micro-continent that originated from Gondwana (e.g. Collins et al., 2003; Sengor, 1979; Stampfli et al., 2013; Xiao et al., 2010). Paleogeographic reconstruction of the micro-continents in the Pangea assembly during the Paleozoic is more complicated and challenging than that of large continents due to complex deformation history, relatively poor exposure, and confusing information accessible. For example, the Qiangtang terrane as part of the Cimmerian continent is traditionally regarded as a single block that drifted and accreted to the southern margin of the North China/Tarim continent during the closure of the Paleotethyan Ocean (e.g. Collins et al., 2003; Stampfli et al., 2013; Yin and Harrison, 2000). However, recent progress shows that the Longmu Co-Shuanghu Paleotethyan suture divided the Qiangtang block into the South Qiangtang terrane with Gondwana affinity and the North Qiangtang terrane with Cathaysian affinity (e.g. Fan et al., 2015, 2017; Li et al., 2006; Li et al., 2018; Li and Zheng, 1993; Zhai et al., 2016; Zhang, 2001; Zhang et al., 2006a, 2006b, 2012, 2018). To the southeast, the Indochina terrane was once treated as an isolated micro-continent (Carter et al., 2001; Collins et al., 2003; Stampfli et al., 2013), but recent studies attested it to be part of the Qamdo continent (e.g. Faure et al., 2014; Metcalfe, 2013; Wang et al., 2016). Moreover, the Central Pamir, North Qiangtang, Simao, and Indochina continental blocks made up a ribbon-like micro-continent (named as Pamir-Qamdo continent for convenience in this paper) that was bounded by the Rushan-Pshart, Longmu Co-Shuanghu, and

* Corresponding author.
E-mail address: 948117360@qq.com (S. Wang).

https://doi.org/10.1016/j.lithos.2021.106520
Received 28 June 2021; Received in revised form 19 October 2021; Accepted 22 October 2021
Available online 28 October 2021

Changning-Menglian sutures to the south and the Tanymas, Jinshajiang, and Song Ma sutures to the north; both suture belts belong to the Paleotethyan Ocean (Fig. 1a) (e.g. Angiolini et al., 2013; Robinson, 2015; Tang et al., 2020; Wang et al., 2019, 2020). Thus, it seems that the Cimmerian and the Pamir-Qamdo ribbon-like micro-continents gradually drifted and accreted to the Laurasia continent during the closure of the Paleotethyan Ocean.

Although the eastern Cimmerian and Pamir-Qamdo continents are all typical tectonic blocks comprised by different types of crystalline basement overlain by sedimentary cover sequences, with Permian-Triassic volcanic arcs along their boundaries (e.g. Cui et al., 2006; Fan et al., 2015, 2017; Li et al., 2006; Li et al., 2018; Li et al., 2019; Li and Zheng, 1993; Metcalfe, 2013; Wang et al., 2019, 2020; Xia et al., 2006; Zhang et al., 2012; Zhang and Tang, 2009), uncertainties still exist regarding the relationships among the micro-continents during the Paleotethyan Ocean evolution. First, ophiolite mélange has not been found for ~700 km long between the Longmu Co-Shuanghu suture and the Changning-Menglian suture in eastern Tibet (Fig. 1a); such a knowledge gap challenges the proposed connection between the two sutures (e.g. Fan et al., 2015, 2017; Jian et al., 2009a, 2009b; Li et al., 2006, 2018; Tang and Zhang, 2014; Wang et al., 2013, 2019; Zhai et al., 2016; Zhang et al., 2018; Zhang and Tang, 2009). This is a reason why the Longmu Co-Shuanghu ophiolite suite was treated as exotic rocks from the Jinshajiang suture in previous studies (e.g. Kapp et al., 2000; Pullen et al., 2008). Moreover, the architecture of the Longmu Co-Shuanghu suture is different from that of the Changning-Menglian suture, in which the Jinghong-Nan suture, regarded as a back-arc basin of the Changning-Menglian-Inthanon suture, is found east of the Lincang-Sukhothai volcanic belt (Figs. 1a, 10b) (e.g., Feng et al., 2002; Metcalfe, 2013; Sone and Metcalfe, 2008), whereas there is no such a tectonic unit reported by the studies on the Longmu Co-Shuanghu suture (e.g. Li et al., 2006; Zhai et al., 2016; Zhang et al., 2006a, 2006b). In addition, detailed information about some micro-continent basements, such as the Simao-Qamdo and the South Qiangtang terranes, is unclear due to either the coverage of Mesozoic strata or structural overprint.

After the discovery of eclogite-blueschist, ophiolite suite, and volcanic belt along the Longmu Co-Shuanghu suture in central Tibet (Li et al., 2006, 2009; Zhang, 2001; Zhang et al., 2006a, 2006b; Zhang and Tang, 2009;), Li et al. (2009) synthesized the work on the North Lancangjiang tectonic (or volcanic) belt around eastern Tibet and suggested that the North Lancangjiang tectonic (or volcanic) belt is the eastern segment of the Longmu Co-Shuanghu suture based on the different features of the basement (Fig. 1b), Carboniferous-Permian strata, and the Indosinian volcanic belt between the Qamdo and the South Qiangtang terranes. Several geochronological and geochemical studies on granites also suggested the North Lancangjiang tectonic (or volcanic) belt be the eastern segment of the Longmu Co-Shuanghu suture (e.g. Peng et al., 2015; Tao et al., 2014; Wang et al., 2019). Recently, high-pressure minerals found around the Dingqing area imply block subduction and collision related to the closure of the Paleotethyan Ocean (Zhang et al., 2018). This is new evidence for Longmu Co-Shuanghu suture in eastern Tibet. Nevertheless, the lack of ophiolite mélange suite in eastern Tibet remains an outstanding issue in this model.

An ophiolite mélange suite around Bitu town, named after it in eastern Tibet, was described by Wu (2006), who attributed the Bitu ophiolite mélange to be N-MORB suture related to the Paleotethyan Ocean. However, due to intensive shortening of the blocks around the eastern Himalayan syntaxis in the Cenozoic, the Jinshajiang suture is only about 40–60 km from the Bangong-Nujiang suture around the Deqin area (Fig. 1c); Pan et al. (2012) argued that the Bitu ophiolite mélange suite was part of the Bangong-Nujiang suture and the boundary of the Gondwana and the Cathaysian blocks.

Since the Bitu ophiolite is located between the Longmu Co-Shuanghu suture and the Changning-Menglian suture, its tectonic affinity is critical to reconstructing the Paleo−/Meso-Tethyan evolution of eastern Tibet. In this contribution, we present geochronological and geochemical data of the basic rocks from the Bitu ophiolite mélange to better understand the correlation and evolution of the Paleotethyan sutures. Based on the newly obtained data in this paper and previously published data, we attempt to elucidate the tectonic affinity of the Bitu suture zone in the context of the Paleotethyan Ocean in the Paleozoic, which may better constrain the northern boundary of the Cimmerian micro-continents across the present-day Tibetan Plateau.

2. Geologic setting

The Cimmerian block, which includes the Turkey, Iran, Afghan, Qiangtang, Baoshan, and Sibumasu micro-blocks, extends over a distance of >7000 km from the Mediterranean Sea in the west to the Sumatra arc in the east (Fig. 1a). Due to the complex tectonic history of the amalgamated orogenic belts, as well as subsequent widespread Cenozoic intracontinental deformation, correlations of the blocks comprising the Tibetan plateau with those in the Pamir plateau and Southeast Asia remain unresolved. In particular, intense strain localized at the western and eastern Himalayan syntaxis during the Cenozoic has resulted in discussion on whether the Rushan-Pshart Suture (RPS) corresponds to the Bangong–Nujiang suture (BNS), and whether the Longmu Co-Shuanghu suture corresponds to the Changning-Menglian suture (Fig. 1a) (e.g. Angiolini et al., 2013; Lacassin et al., 2004; Metcalfe, 2013; Pan et al., 2012; Schwab et al., 2004).

The strike of the South and North Qiangtang terranes, which are connected with the Baoshan and Simao micro-continents in southeastern Tibet separately, bends from E-W-trending to SE-NW-trending under the continuous indentation of the eastern Himalayan syntaxis in the Cenozoic (Fig. 1a). The stratigraphy and fossil assemblages show a significant difference between the South Qiangtang-Baoshan and North Qiangtang-Simao micro-continents. Paleozoic sedimentary rocks from the South Qiangtang-Baoshan micro-continents are characterized by glaciomarine deposits and cold-water biota, which is a typical feature of Gondwana affinity, whereas those from the North Qiangtang-Simao micro-continents contain abundant warm-water fossils of a Cathaysian affinity (e.g. Fan et al., 2015; Feng et al., 2002; Li and Zheng, 1993; Ueno, 2003; Zhang et al., 2012). The Longmu Co–Shuanghu suture zone between the South and North Qiangtang and the Changning-Menglian suture zone between the Baoshan and Simao micro-continents have been regarded as the main Paleotethyan suture which are all characteristic of ophiolitic mélange, ocean-island basalts (OIB), metasedimentary rocks, and minor chert (e.g. Jian et al., 2008, 2009a, 2009b; Li and Zheng, 1993; Tang and Zhang, 2014; Wu et al., 1995; Zhang et al., 2006a, 2006b; Zhang and Tang, 2009).

Traditionally, the Qiangtang terrane in the eastern Tibetan plateau is subdivided into several units, including the Jinshajiang volcanic belt, the Mangkang Mesozoic sediment belt, the North Lancangjiang volcanic belt, the Zuogong metamorphic belt, and the Basu Mesozoic sediment belt (Fig.1b; Pan et al., 2012). The strata between the Jinshajiang suture and the Bangong-Nujiang suture in the eastern Tibetan plateau is characterized by widespread Mesozoic sediments; outcrop of the basement rocks (Mainly 2.4–1.8 Ga) is only found so far in the northeast of the study area along the Jinshajiang suture (He et al., 2011). The North Lancangjiang volcanic belt is developed in the middle of the Jinshajiang volcanic belt and the Bangong-Nujiang suture (Fig. 1b). Previous studies indicated I- and S-type granites related to the subduction of the Paleotethyan Ocean were developed in the North Lancangjiang volcanic belt, and suggested the Qiangtang terrane in eastern Tibet be divided into two parts as that in central Tibet (e.g. Peng et al., 2015; Tao et al., 2014; Wang et al., 2019). Regretfully, there is no robust ophiolite mélange information to directly support this deduction. In this paper, we show the newly found ophiolite mélange named Bitu suture in slates and carbonates of the Zuogong metamorphic belt in eastern Tibet (Fig. 1c).

Due to the remote location and harsh conditions, the ~3-km-thick Middle Carboniferous strata in the Zuogong metamorphic belt have not been classified into or given any specific formation or group names

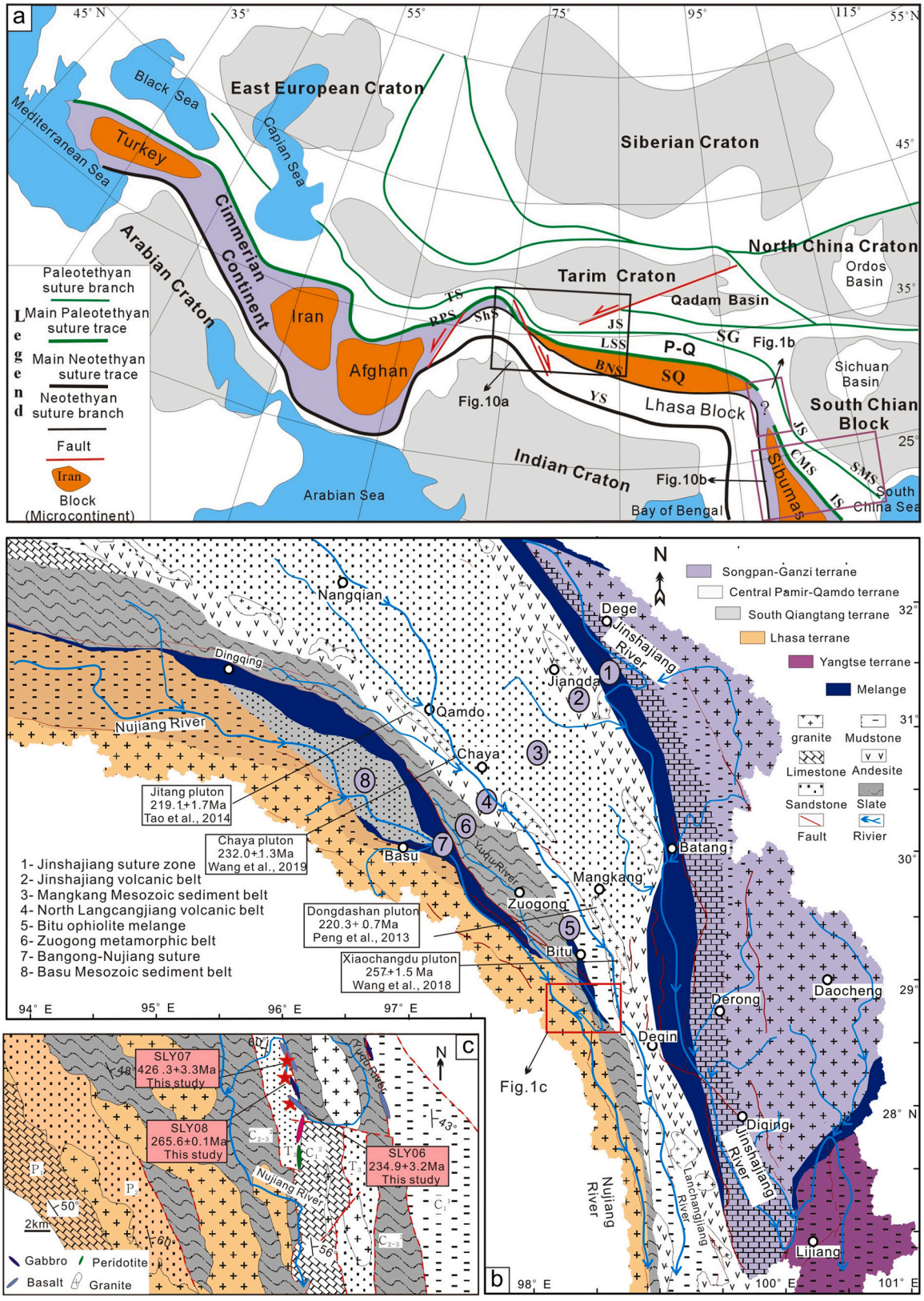

Fig. 1. a) A sketch map of the Paleotethyan sutures in Himalayan-Tibetan orogenic belt and its neighborhood; b) Simplified geologic map of the eastern Tibet (after Xizang BGMR, 1993), part of geochronological data in the study area also shown; c) Simplified geologic map that shows the sites of the samples collected in this paper. Abbreviations: BNS- Bangong-Nujiang suture; CMS- Changning-Menglian suture; IS- Inthanon suture; JS- Jinshajiang suture; KS- Kudi suture; LSS- Longmu Co-Shuanghu suture; RPS- Rushan-Pshart suture; P-Q - Central Pamir-north Qiangtang-Simao-Indochina; ShS- Shyok suture; SMS- Song Ma suture; SG- Songpan-Ganzi flysch belt; SQ-south Qiangtang; TS- Tanymas suture; YS- Yalong–Indus suture.

(BGMRX, 1993). Our fieldwork found that the Carboniferous strata are composed of low-grade metamorphic slate, phyllite, and black limestone with coral fossils, in which serpentinite, gabbro, basalt, and minor abysmal radiolarian silica rock are found (Figs. 1c, 2). These rocks were first reported as the Bitu ophiolitic mélange by Wu (2006); however, no age constraint is available. It commonly occurs as isolated blocks and/or mélanges in fault contact with the Carboniferous strata (Figs. 2a-2b). The peridotites are extensively serpentinized, and most olivine and orthopyroxene have been completely replaced by serpentine (Fig. 2a, g, h). The gabbros are isotropic, most of which have experienced some degrees of epidotization and chloritization, and pyroxene is partly replaced by actinolite (Fig. 2i). The basalts commonly occur as weakly deformed blocks (Figs. 2j-2l).

3. Analytical methods

Three samples from the Bitu ophiolite mélange belt were prepared for zircon U—Pb LA-ICP-MS dating (Fig. 1c). Zircons were separated using conventional heavy-liquid and magnetic techniques. Pure zircon grains were selected using a binocular microscope. Representative grains were placed into an epoxy resin and ground down by about half to expose the zircon interior, before U—Pb dating. Before and after the dating, zircon grains were examined and photographed in transmitted and reflected light under the polarized microscope, together with cathodoluminescence (CL) images, in order to determine the crystalline shape, inner structure, and dating position.

Zircon U—Pb dating was undertaken using a New Wave UP193FX

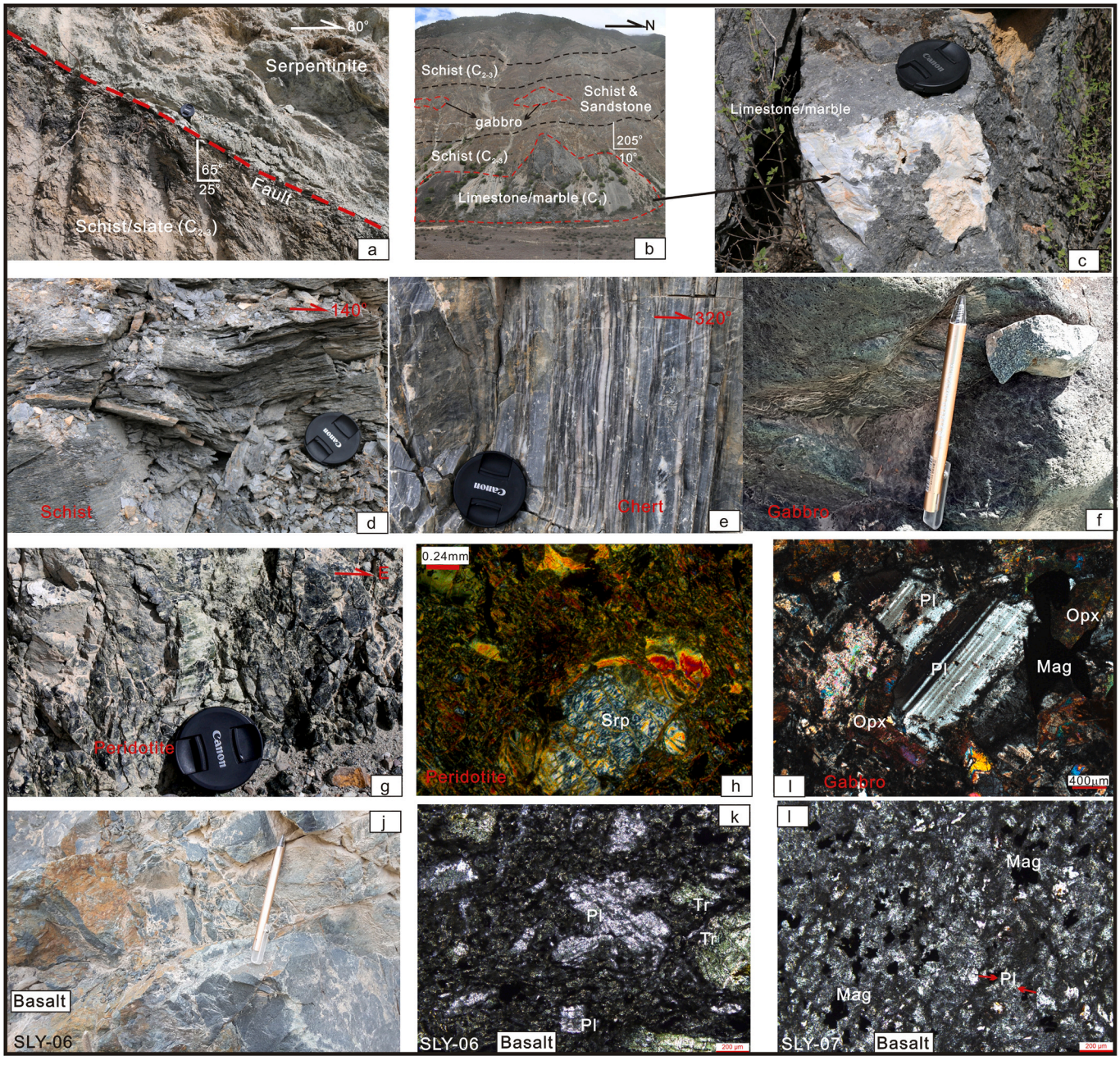

Fig. 2. Rocks from the Bitu mélange zone: 2a- fault contact between serpentinites and schist; 2b) gabbro mass in schist; 2c) limestone; 2d- slate and Schist; 2e-chert; 2f- gabbro; 2 g- Serpentinized peridotite; 2 h- Serpentinized peridotite under crossed polarizers; 2i: gabbro under crossed polarizers; 2j: basalt; 2 k- basalt under single polarizers (SLY06); 2 L- basalt under single polarizers (SLY07); Abbreviations: Mag-magnetite; Opx- orthopyroxene; Pl- plagioclase; Qtz- quartz; Srp- serpentine;. Tr- Tremolite.

Excimer LA system coupled with an Agilent 7500a ICP–MS instrument, at the Key Laboratory of Continental Collision and Plateau Uplift, Institute of Tibetan Plateau Research, Chinese Academy of Sciences (CAS), Beijing, China. These analyses used a 36-μm diameter laser beam and a 45 s ablation time. Helium was used as the carrier gas within the ablation cell to enhance the transport efficiency of the ablated materials. Raw count rates for ^{29}Si, ^{204}Pb, ^{206}Pb, ^{207}Pb, ^{208}Pb, ^{232}Th, and ^{238}U were collected for age determinations, with U, Th, and Pb concentrations as well as the concentrations of some other selected trace elements being calibrated using ^{29}Si as an internal standard and a NIST SRM 610 silicate glass standard as reference material. $^{207}Pb/^{206}Pb$, $^{206}Pb/^{238}U$, $^{207}Pb/^{235}U$, and $^{208}Pb/^{232}Th$ isotopic ratios and age estimates were calculated using the Macquarie University GLITTER 4.0 program and were corrected using the 91,500 zircon as an external standard. Weighted average age calculations and concordia diagram construction were undertaken using Isoplot/Ex version 3.0 (Ludwig, 2003). Age calculations were based on U decay constants of $^{235}U = 9.8454 \times 10^{-10}$/yr and $^{238}U = 1.55125 \times 10^{-10}$/yr (Ludwig, 2003), and common Pb corrections were made using the approach of Andersen (2002).

In situ zircon Lu—Hf isotopic analyses were conducted using a New Wave UP213 LA system coupled with a Neptune multicollector (MC)–ICP–MS instrument at the State Key Laboratory for Mineral Deposits Research, Nanjing University, Nanjing, China. The in situ zircon LA–ICP–MS Hf isotopic analysis used a beam size of 60 μm and a laser pulse frequency of 8 Hz. Details of the analytical approaches used and the methods used to correct for the interference of ^{176}Yb on ^{176}Hf are given in Hou et al. (2007). A ^{176}Lu decay constant of 1.865×10^{-11}/yr was used to calculate initial $^{176}Hf/^{177}Hf$ ratios, and the chondritic values of $^{176}Lu/^{177}Hf = 0.0332$ and $^{176}Hf/^{177}Hf = 0.282772$ reported by Blichert-Toft and Albarede (1997) were used to calculate $\varepsilon_{Hf}(t)$ values. Single-stage model ages (T_{DM1}) were calculated using a depleted mantle reservoir with a present-day $^{176}Hf/^{177}Hf$ value of 0.28325 and a $^{176}Lu/^{177}Hf$ value of 0.0384, whereas two-stage Hf model ages (T_{DM2}) were calculated using a $^{176}Lu/^{177}Hf$ value of 0.015 for the average continental crust (Griffin et al., 2000). A GJ-1 standard zircon was used for external standardization. $\varepsilon_{Hf}(t)$ values were calculated using a decay constant of ^{176}Lu of 1.865×10^{-11}/yr, and all individual Hf isotopic analyses were located within the previously ablated U—Pb analysis pits.

Eighteen basaltic samples were chosen for whole-rock major, trace, and rare earth element analysis. Prior to analyses, fresh and weakly deformed fragments from these samples were selected and powdered to <20 μm in size using an agate mill. Major element analyses were undertaken at the Institute of Geology and Geophysics, CAS, Beijing, China, using a Phillips PW XRF-2400 X-ray fluorescence spectrometer, yielding an analytical uncertainty of <5% (±1). The accuracy and precision of the data were assessed using international standard reference GSR-3. The related data are presented in Appendix Table 3. Trace element concentrations, including those of the rare earth elements (REEs), were determined using solution ICP–MS at the Institute of Tibetan Plateau Research, Beijing, China. Analytical results for standard AGV-2 are also presented in Appendix Table 3. Details of the operating conditions for the ICP–MS instrument and the data reduction approaches used are given in Liu et al. (2008) with <5% uncertainties on all trace element concentrations.

4. Results

4.1. Zircon U—Pb LA-ICPMS ages

Three samples were selected for zircon U—Pb dating, including one isotropic gabbro sample (SLY08, location: 28°35′58″N, 98°27′09″E) and two basalt samples (SLY06, location: 28°44′24″N, 98°26′05″E; SLY-07, location: 28°43′19″N, 98°26′20″E). All zircon grains from the three samples have similar crystal forms. They are prismatic, euhedral, transparent, and colorless. Most zircon grains are 50–100 μm long and have length-to-width ratios of 1–3. The CL images display weak oscillatory zoning (Fig. 3), and most zircon grains have Th/U ratios >0.1 (Appendix Table 1). Therefore, the zircon crystals are most likely of magmatic origin (Hoskin and Schaltegger, 2003). The U—Pb age results are given in Appendix Table 1, and are plotted in the concordia diagrams in Fig. 3. Analysis on 25 zircons collected from basalt SLY06 yield concordant $^{206}Pb/^{238}Pb$ ages from 1449 Ma to 226 Ma with a cluster at 234.9 ± 3.2 Ma ($n = 8$, mean square of weighted deviates [MSWD] = 1.7) (Appendix Table 1). In contrast, 20 analyses on zircons from basalt SLY07 show a cluster at 426.3 ± 3.3 Ma ($n = 6$, MSWD = 0.58) and other xenolithic zircon grains yielded ages ranging from ~2300 Ma to ~660 Ma (Appendix Table 1). The isotropic gabbro samples yield a weighted mean $^{206}Pb/^{238}U$ age of 265.6 ± 0.1 Ma (SLY08: $n = 21$, MSWD = 0.48).

4.2. Zircon Lu—Hf isotopic analysis

The three samples dated above (SLY-06, −07, −08) are selected for in situ zircon Lu—Hf isotopic analysis. The results are plotted in Fig. 4 and listed in Appendix Table 2.

Eight zircon grains with a mean U—Pb age of 234.9 Ma from sample SLY06–1 yield initial $^{176}Hf/^{177}Hf$ ratios of 0.282284–0.282722 and $\varepsilon_{Hf}(t)$ values of −16.4 to +3.3, with a weighted mean $\varepsilon_{Hf}(t)$ value of −8.0. Their Hf crustal one-stage model ages (T_{DM1}) fall between 750 Ma and 1553 Ma, with a mean of 1230 Ma.

Seven zircon grains whose mean U—Pb age is 426.3 Ma from sample SLY07–1 yield initial $^{176}Hf/^{177}Hf$ ratios of 0.282207–0.282633 and $\varepsilon_{Hf}(t)$ values of −10.8 to +4.1, with a weighted mean $\varepsilon_{Hf}(t)$ value of −4.5. Their Hf crustal one-stage model ages (T_{DM1}) fall between 894 and 1494 Ma, with a mean of 1238 Ma.

Seventeen analyses of zircon grains from sample SLY08–1 yield initial $^{176}Hf/^{177}Hf$ ratios of 0.282619–0.282947 and $\varepsilon_{Hf}(t)$ values of +0.1 to +12.1 with a mean value of +4.3. The corresponding Hf crustal two-stage model ages (T_{DM2}) range from 693 to 1286 Ma, with a mean age of 1031 Ma.

4.3. Major- and trace-element geochemistry

Basalt samples (SLY06 series) have $SiO_2 = 46.7$ wt%–50.4 wt%, $TiO_2 = 2.5$ wt%–3.3 wt%, $Al_2O_3 = 11.3$ wt%–14.0 wt%, $Fe_2O_{3T} = 10.15$ wt%–12.68 wt%, and MgO = 5.2 wt%–8.2 wt% (Appendix Table 3). The samples plot in the gabbro field in the ($Na_2O + K_2O$) versus SiO_2 diagram (Fig. 5A; Middlemost, 1994), and fall in the tholeiitic field in the whole rock alkali ($Na_2O + K_2O$)–FeOt–MgO (AFM) diagram (Fig. 5B; Irvine and Baragar, 1971). Chondrite-normalized REE and primitive-mantle–normalized trace element concentrations for the basalts and gabbro Chaya diorites are shown in Fig. 6A and B. The average of the total REE (ΣREE) of basalt sample SLY06 is about 141 ppm, and the chondrite-normalized REE patterns of SLY06 series show high light REE (LREE) concentrations and relatively low heavy REE (HREE) with a mean LREE/HREE ratio of 2.4, with minor to no Eu anomalies (Fig. 6A). In the spidergrams (Fig. 6B), the SLY 06 series basaltic rocks display enrichment in large-ion lithophile elements (LILE) such as Rb, Ba, and K, and no depletion in high field strength elements (HFSE) such as Nb, Ta, Zr, Hf, and Ti. In general, these rocks have trace element distribution patterns similar to those of typical ocean island basalts (OIB) but substantially different from those of normal mid-ocean ridge basalts (MORB). This conclusion is also supported by the ratio of incompatible elements ratio $(La/Sm)_N > 1$. In the Bowen diagrams (Fig. 7), positive correlations with Al_2O_3, CaO, Cr, and Ni, and negative correlations with Fe_2O_{3t}, TiO_2, $K_2O + Na_2O$, and P_2O_5 are observed.

Basalt samples (SLY07 series) have $SiO_2 = 45.6$ wt%–47.8 wt%, $TiO_2 = 1.7$ wt%–1.9 wt%, $Al_2O_3 = 13.4$ wt%–13.9 wt%, $Fe_2O_{3T} = 13.1$ wt%–13.8 wt%, and MgO = 6.7 wt%–7.4 wt% (Appendix Table 3). The samples plot in the gabbro field in the ($Na_2O + K_2O$) versus SiO_2 diagram (Fig. 5A; Middlemost, 1994), and fall in the tholeiitic field in the whole rock alkali ($Na_2O + K_2O$)–FeOt–MgO (AFM) diagram (Fig. 5B; Irvine and Baragar, 1971). The total ΣREE of basalt sample SLY07

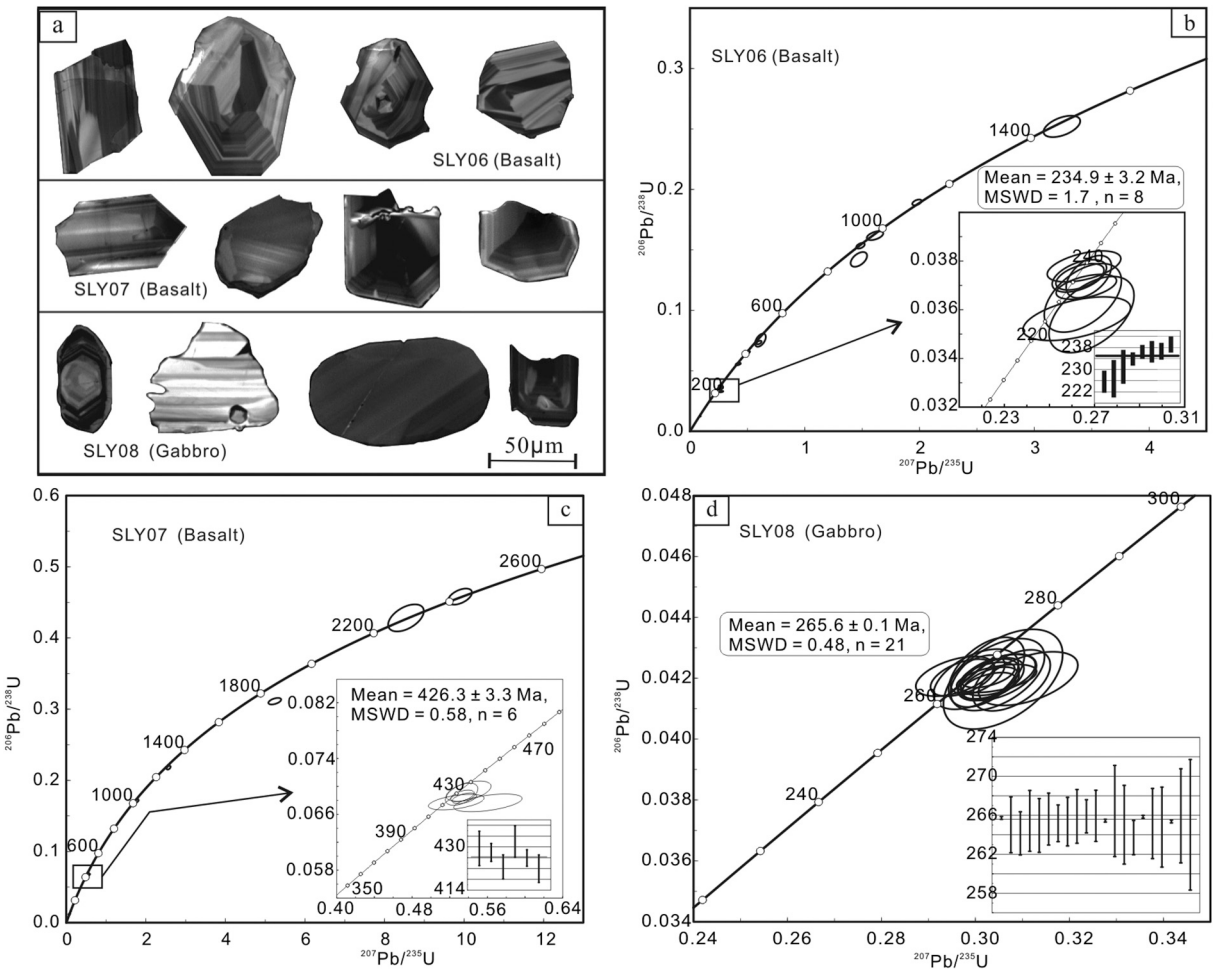

Fig. 3. Concordia diagram of zircon LA-ICPMS U—Pb dating for basaltic rocks. MSWD: mean square of weighted deviation.

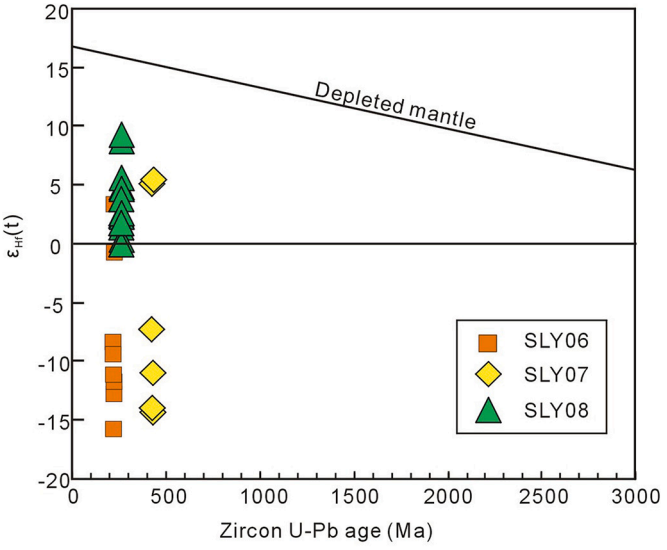

Fig. 4. $\varepsilon_{Hf}(t)$ vs. U—Pb ages for granites of the basaltic rocks. Hf isotopic compositions of chondrite and depleted mantle are from Blichert-Toft and Albarede (1997).

(~102 ppm) is relatively lower than that of the SLY06 series. The chondrite-normalized REE patterns of the SLY07 series show slightly lower LREE concentrations relative to HREE, with a mean LREE/HREE ratio of 0.7 and minor to no Eu anomalies (Fig. 6A). In the spidergrams (Fig. 6B; Sun and McDonough, 1989), the SLY 07 series basaltic rocks are enriched in U, Th, and Pb, and depleted in Ta, Nb, and Sr. The REE and trace-element characters of sample SLY07 series are comparable with those of either normal mid-ocean-ridge basalts (N-MORB) or enriched mid-ocean-ridge basalts (*E*-MORB), the incompatible element ratio ($[La/Sm]_N < 1$) also supports this conclusion.

The isotropic gabbro samples (SLY08 series) show SiO_2 = 48.7 wt%–49.8 wt%, TiO_2 = 1.0 wt%–1.3 wt%, Al_2O_3 = 15.0 wt%–15.7 wt%, Fe_2O_{3T} = 10.0 wt%–11.1 wt%, MgO = 6.4 wt%–7.3 wt% and total alkalis ($Na_2O + K_2O$) = 3.0 wt%–3.1 wt% (Table 1). The high SiO_2 contents are consistent with their high modal content of plagioclase. They fall in the gabbro field in the ($Na_2O + K_2O$) versus SiO_2 diagram (Fig. 5A; Middlemost, 1994), and show a tholeiitic trend in the AFM diagram (Fig. 5B; Irvine and Baragar, 1971). The average of total ΣREE of gabbro SLY08 samples is about 131 ppm, and the chondrite-normalized REE patterns of the SLY08 series show high LREE concentrations and relatively low HREE with a mean LREE/HREE ratio of 1.5, with minor to no Eu anomalies (Fig. 6A). The REE patterns of isotropic gabbros (Fig. 6A and B) are uniform and enriched in LREEs. In spidergrams, the isotropic gabbros show are enriched in large ion lithophile elements (e.g., Rb, Eu, and Pb) and depleted in high field strength elements (e.g., Ta, Nb, and Ti). They are comparable to those of E-MORB (Sun and McDonough, 1989). In the Bowen diagram (Fig. 7), the gabbroic rocks show similar features to those of basalt samples from the SLY06 and SLY07 series.

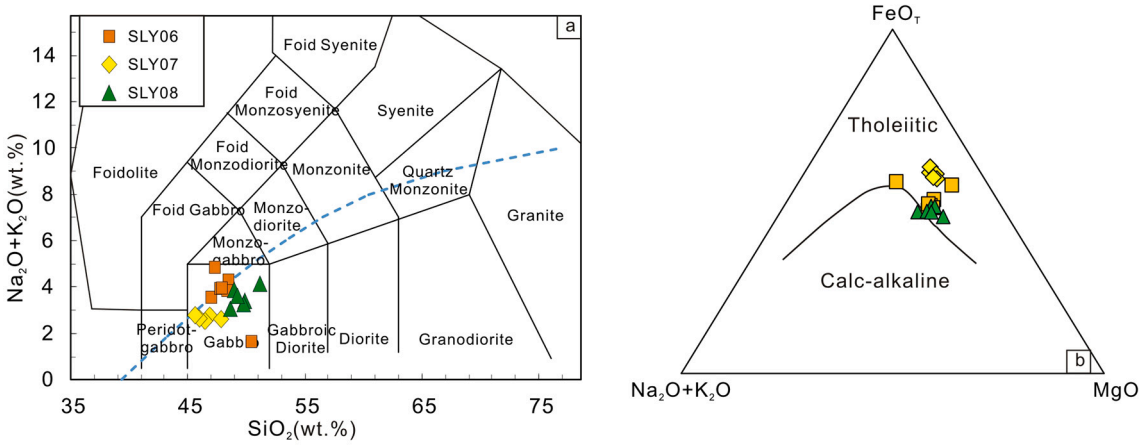

Fig. 5. Diagrams showing the geochemical compositions of the Tash and Tahman granitoids. (a) ($K_2O + Na_2O$) vs. SiO_2 diagram (after Middlemost, 1994) showing the classification of the Tash and Tahman granitoids; (b) ($Na_2O + K_2O$)-FeO_T -MgO (in wt%; after Irvine and Baragar, 1971) diagrams indicating magma source characteristics for the basaltic rocks from the Bitu melange.

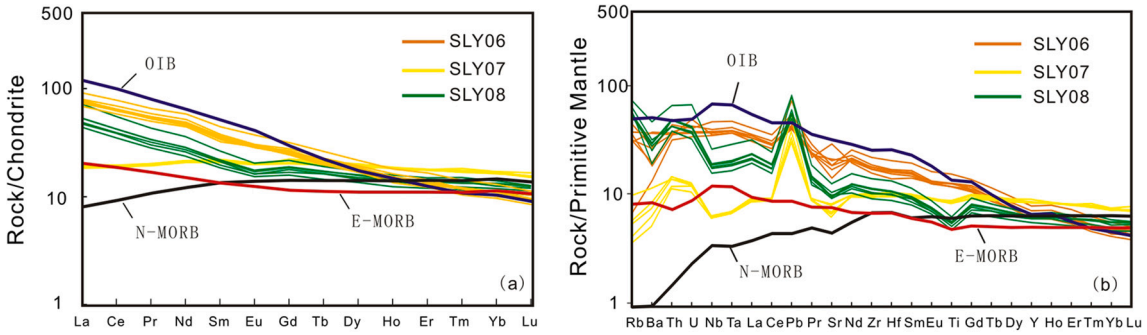

Fig. 6. Chondrite-normalization REE patterns and primitive mantle-normalized trace element diagrams for the basaltic rocks. Chondrite-normalization data are from Boynton (1984). Primitive mantle-normalized data are from Sun and McDonough (1989).

5. Discussion

5.1. Petrogenesis and magma source

Due to the unsaturation of Si in mafic magma, it is usually regarded that zircons are unlikely to crystallize directly from mafic magma, and the zircons in basalt are xenocrysts entrained during either the ascent or emplacement of the magma on the surface (e.g. Boehnke et al., 2013; Corfu et al., 2003). Thε$_{Hf}$(t) values of the zircons from basalts SLY06 and SLY07 ranging from −16.4 to +4.2 are indicative of a xenocryst origin, and their ages only represent an upper limit of the basalt. Additionally, the 234.9-Ma zircon age obtained from the basalt SLY06 is similar to the granitic ages in this tectonic belt (e.g. Peng et al., 2015; Wang et al., 2019), and the 426-Ma age from the basalt SLY07 is similar to the mafic rock ages from the Longmu Co-Shuanghu suture (e.g. Wang et al., 2015; Zhai et al., 2016). The existence of 265-Ma gabbro, 426-Ma and 234-Ma basalt, serpentinites, and cherts all in the so-called "Carboniferous strata" (BGMRX, 1993) indicates that the "Carboniferous" strata are a suite of ophiolite mélange rather than a sediment unit. The protoliths of the "Carboniferous" schist and phyllite are mainly derived from fine-grained segments of the Bouma Sequence and experienced low-grade metamorphism during later orogeny. The 426 Ma - 234 Ma basalt/gabbro are coeval with the evolution of the Paleotethyan Ocean in the Tibetan Plateau (e.g. Jian et al., 2009a, 2009b; Wang et al., 2013; Zhai et al., 2016; Zhang et al., 2013), therefore, we attribute these samples to be part of the Paleotethyan suture in eastern Tibet.

According to the rock association, petrography, geochemistry, and tectonic setting, ophiolites can be divided into two types: SSZ (supra-subduction zone) type that is related to subduction, and MOR (mid-ocean ridge) type that is not related to subduction (Dilek and Furnes, 2011). Ophiolites related to subduction (SSZ type) are mainly formed in island arc, forearc, and back-arc basins. Ophiolites related to the MOR type can be further divided into continental margin type, mid-ocean ridge type, and mantle column type. The three series of basic rocks in this study are attributed to tholeiitic rocks, and have certain similarities in geochemical characteristics; nevertheless, their different diagenetic age and different geochemical features indicate distinct petrogenesis and magma sources.

5.1.1. Petrogenesis and magma source of basalt SLY06

The mean content of Mg# from SLY06 samples is about 56, which is less than the average content of the original mantle magma (68–75), indicating that the magma experienced a certain degree of crystallization and contamination. The SLY06 samples show LREE enrichment and HREE flattening on chondrite-normalized REE patterns with a mean LREE/HREE ratio of 2.4, $(La/Yb)_{PM}$ ratio of about 7.53, and $(Ce/Yb)_{PM}$ ratio of about 6.43, the latter two of which are much higher than those of N-MORB (0.59, 0.68) and *E*-MORB (1.91, 1.76), respectively. Moreover, the SLY 06 series basaltic rocks are enriched in large ion lithophile elements (LILEs; e.g., Rb, Pb and Eu) with the $(La/Sm)_{PM} = 2.2$, which supports that the SLY06 samples are part of the within-plate alkali basalt (WPA) or OIB (Niu, 2009). Basalt SLY06 samples show no Eu anomaly ($Eu/Eu^* = 0.97–1.01$), thus there is no obvious separation crystallization of plagioclase. High field strength elements (HFSEs) (such as Zr, Hf, Nb, Ta, Ti, Y) are less active and have good stability in the process of metamorphism, and are reliable indicators for studying the genesis and

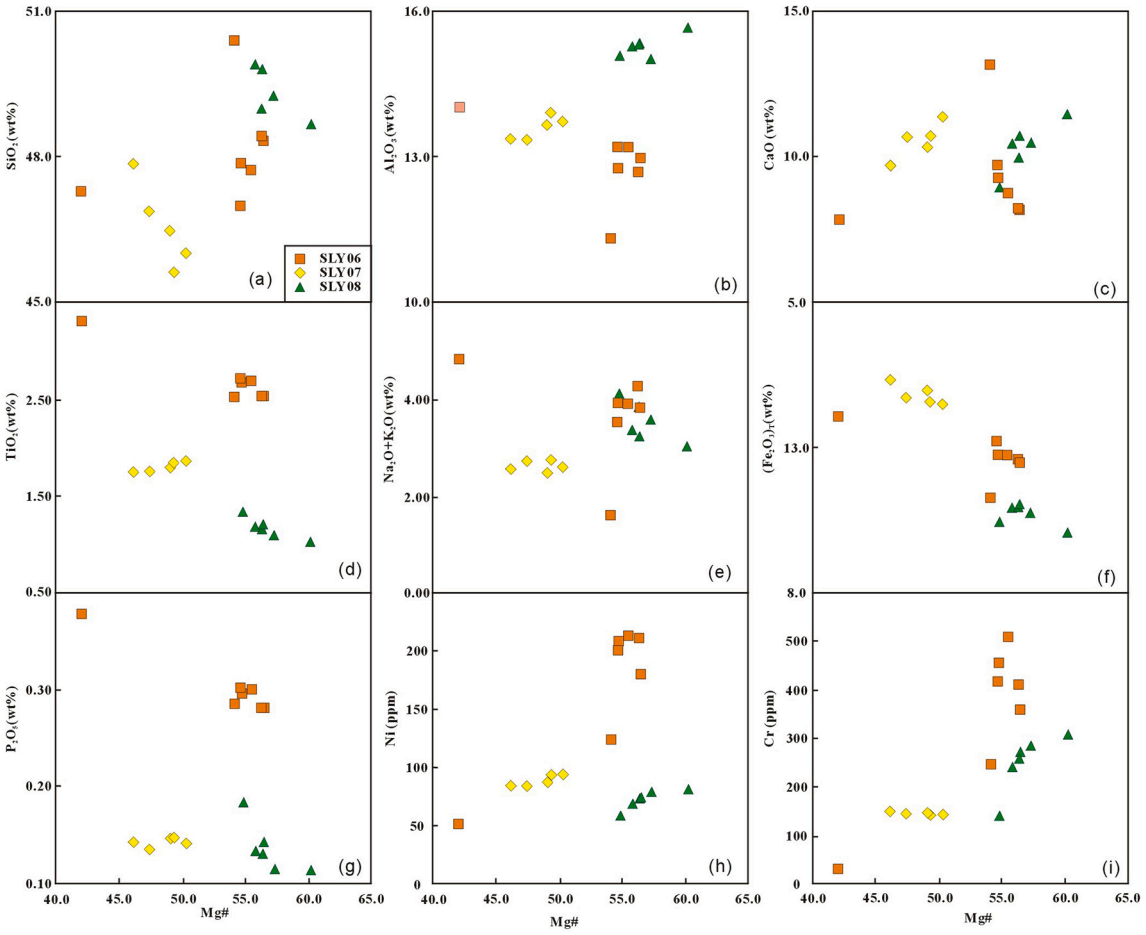

Fig. 7. Bowen variation diagrams for the Bitu mélange, eastern Tibetan Plateau. (Mg# = 100 × Mg/(Mg + Fe2+).

Table 1
Terrane and suture correlations among the Pamir, Tibetan Plateau, and Southeast Asia areas.

Regions / Continents	Pamir	West Kunlun	Central Tibet	East Tibet	SE Asia
Laurasia	**North Pamir**	**South Kunlun – North Kunlun**	**Songpan-Ganzi**		South China
Paleotethyan suture	Tanymas	Mazha-Kangxiwa	Jinshajiang		Song Ma
Pamir-Qamdo	Central Pamir	Tianshuihai	North Qiangtang	Qamdo-Simao	Indochina
Paleotethyan suture	Rushan-Pshart	Longmu Co-Shuanghu		Changning-Menglian	Inthanon
Cimmerian	South Pamir -Karakorum	South Qiangtang		Baoshan	Sibumasu
Mesotethyan suture	Shyok	Bangong-Nujiang			Gaoligong
Gondwana	Hindu-Kush	Lhasa		Tengchong	West Burma

source properties of magma (Pearce, 1982). Mean Zr content in SLY06 basalts is about 200 ppm, and Hf content is about 5.05 ppm, which are similar to those in WPA (149–213 ppm, 3.44–6.36 ppm, respectively) and much larger than those in MORB (90–96 ppm, 2.4–2.93 ppm, respectively). In the 2Nb-Zr/4-Y diagram, all samples fall in the within-plate tholeiitic basalt field (AII); in V-Ti/1000 diagram, all samples fall in the OIB field; and in the Th/Yb-Nb/Yb diagram (Fig. 8c), all samples fall in the overlapping field of *E*-MORB and OIB. All the above

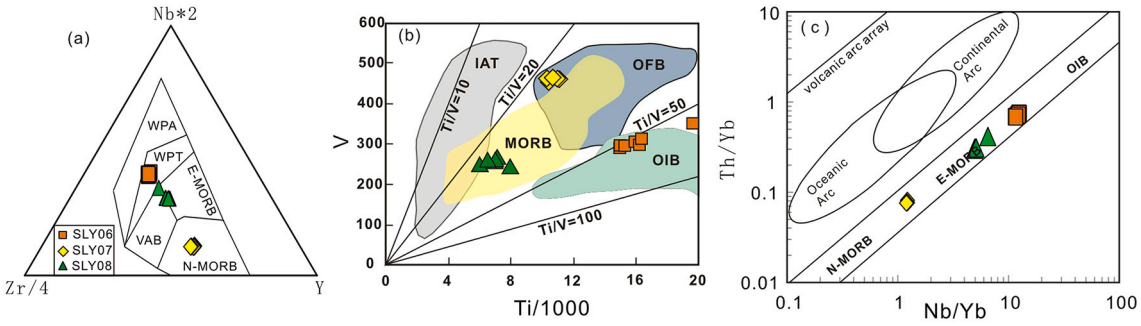

Fig. 8. (A) Nb-Zr-Y diagram after Meschede (1986), (B) V vs. Ti/1000 diagram after Shervais (1982) and Rollinson (1993), and (C) Th/Yb vs. Nb/Yb diagram after Pearce (2008) for basalts and gabbros of the Bitu ophiolitic mélange, eastern Tibetan Plateau. Abbreviations: *E*-MORB- enriched MORB; FAB- fore-arc basalt; IAT- island-arc tholeiite; MORB-mid-ocean ridge basalt; N-MORB-normal MORB; OFB- oceanic flood basalt; OIB- oceanic island basalt; VAB- volcanic-arc basalt; WPA-within-plate alkali basalt; WPT- within-plate tholeiite.

characteristics drive us to prefer the interpretation of an OIB origin for the samples. In particular, the zircon from the SLY06 basalts exhibits a wide range of initial Hf isotope ratios (ε_{Hf} (t) = −16.4 to +3.3), with the corresponding T_{DM1} of 0.75–1.56 Ga. The ε_{Hf} (t) values are lower than that from MORB, and the T_{DM1} is older than the timing of zircon growth, inherited zircon was also found. These characteristics of sample SLY06 suggest that the source of the basalt is the metasomatic mantle, and the basalt SLY06 originated in a post-orogenic extensional continental environment (Fig. 9b).

5.1.2. *Petrogenesis and magma source of basalt SLY07*

The mean Mg# from SLY07 samples is about 51, which is less than the average content of the original mantle magma (68–75), indicating that the magma experienced a certain degree of crystallization and contamination. The SLY07 samples show LREE is flatter than HREE on chondrite-normalized REE pattern with mean LREE/HREE ratios <1, $(La/Yb)_{PM}$ ratios of about 1.20, and $(Ce/Yb)_{PM}$ ratios of about 1.91; the latter two of which is between those of N-MORB (0.58, 0.68) and E-MORB (1.91, 1.76), respectively. Moreover, the SLY07 series basaltic rocks show $(La/Sm)_{PM}$ = 0.9, which is less than 1, indicating that the SLY07 samples are part of MORB. Basalt SLY07 samples show no Eu anomalies (Eu/Eu* = 0.93–0.97), indicating no obvious separation crystallization of plagioclase. The mean Zr content is about 107 ppm, and Hf content is about 3.01 ppm, which are much smaller than those in WPA (149–213 ppm, 3.44–6.36 ppm, respectively) and close to those of MORBs (90–96 ppm, 2.4–2.93 ppm, respectively; Pearce, 1982). In the 2Nb-Zr/4-Y diagram (Fig. 8a), all samples fall in the N-MORB field; in the V-Ti/1000 diagram (Fig. 8b), all samples fall in the overlapped field of MORB and OFB (ocean floor basalt); and in the Th/Yb-Nb/Yb diagram (Fig. 8c), all samples fall in the MORB field. These features favor the possibility that the samples originated from MORB. Also, zircon U—Pb age of SLY07 is around 426 Ma, and zircon in situ Lu—Hf data exhibit a wide range of initial Hf isotope ratios (ε_{Hf} (t) = −10.8 to +4.1), with the corresponding T_{DM1} of 894–1466 Ma. Inherited zircons are also found. The information above indicates that the mantle-derived magma was contaminated by ancient crustal materials, and suggests that the SLY07 basalts should be associated with the opening stage of the Paleotethyan Ocean (e.g. Jian et al., 2009a, 2009b; Peng et al., 2015; Wang et al., 2013; Zhai et al., 2016).

5.1.3. *Petrogenesis and magma source of gabbro SLY08*

The mean Mg# of SLY08 samples is about 59, which is less than the average content of the original mantle magma (68–75), indicating that the magma experienced a certain degree of crystallization and contamination. Basalt SLY08 samples show slight Eu anomalies (Eu/Eu* = 0.83–0.96), showing no obvious separation crystallization of plagioclase. The SLY08 samples show LREE enrichment and HREE flattening on Chondrite-normalized REE pattern with a mean LREE/HREE ratio of 1.5. Moreover, the SLY08 series basaltic rocks are enriched in large ion lithophile elements (LILEs; e.g., Rb, Pb, and Eu) and depleted in high field strength elements with $(La/Sm)_{PM}$ = 2.5, which supports that the SLY08 samples are OIB-like rocks (Niu, 2009). Their $(La/Yb)_{PM}$ ratios

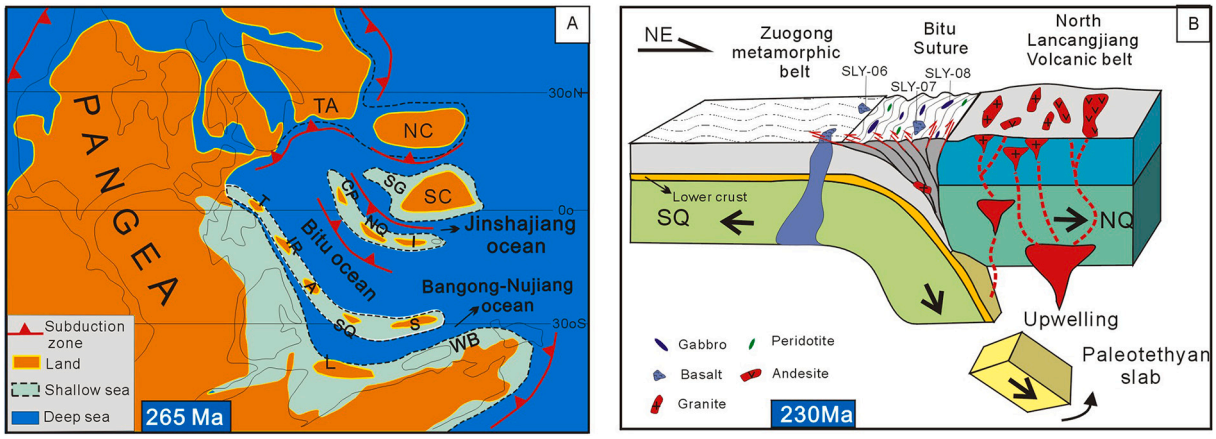

Fig. 9. (a) Paleogeographic reconstructions of the Tethyan region in the Late Permian, showing relative positions of the Pamir and Tibetan blocks, as well as the distribution of land and sea (after Metcalfe, 2013). (b) Geodynamic model of convergence between south and north Qiangtang terranes during the closure of the Paleo-Tethys ocean (after Peng et al., 2015; Zhai et al., 2016; Wang et al., 2018, 2019). (c) Continental blocks: A = Afghan; CP = Central Pamir; I = Indochina; IA = Iran; L = Lhasa; NC = North China; NQ = North Qiangtang; S = Sibumasu; SC=South China; SG = Songpan-Ganzi; SP = South Pamir; SQ = South Qiangtang; T = Turkey; TA = Tarim; WB = West Burma.

are about 4.45, and $(Ce/Yb)_{PM}$ ratios are about 3.56, which are much greater than those of N-MORB (0.59, 0.68, respectively) and *E*-MORB (1.91, 1.76, respectively). The mean Zr content in gabbro SLY08 samples is about 122 ppm, and Hf content is about 3.23 ppm, which are similar to those in WPA (149–213 ppm, 3.44–6.36 ppm, respectively) and much greater than those in MORB (90–96 ppm, 2.4–2.93 ppm, respectively). In the 2Nb-Zr/4-Y diagram (Meschede, 1986), all samples fall in the overlapping field of VAB and N-MORB; in V-Ti/1000 diagram (Shervais, 1982), all samples fall in the overlapped field of MORB and IAT (island–arc tholeiite); and in the Th/Yb-Nb/Yb diagram (Fig. 8c; Pearce, 2008), all samples fall in the overlapped field of OIB and E-MORB. These details exclude the possibility of MORB as the origin of the SLY08 samples. The zircons from the SLY08 basalts exhibit a wide range of initial Hf isotope ratios (ε_{Hf} (t) = 0 to +12.0), with the corresponding T_{DM1} of 693–1286 Ma. The ε_{Hf} (t) values are lower than that of depleted mantle reservoir at 265 Ma, and the T_{DM1} ages are older than the timing of zircon growth. These pieces of information suggest that their source is metasomatic mantle rather than N-MORB-like depleted mantle. Therefore, we suggest that the gabbro SLY08 was derived from an OIB environment.

5.2. *Paleotethyan suture zones between the eastern Cimmerian and Pamir-Qamdo ribbon-like micro-continents*

Our field investigations show that serpentinite, gabbro, basalt, and minor abysmal radiolarian silica fragments are enclosed in the Carboniferous low-grade metamorphic slate, phyllite, and black limestone; these rock assemblages form an ophiolite melange of a suture zone. The slate and phyllite are flysch deposition in abyssal-bathyal. The chronological and geochemical data of the MOR and OIB mafic rocks indicate there is an expanded Paleotethyan Ocean, named Bitu Ocean here, from Late Silurian to Late Permian. Previous studies show the evolution of the Longmu Co-Shuanghu Paleotethyan Ocean is similar to that of the Changning-Menglian ocean and suggest they are as an indivisible whole (e.g. Li et al., 2006; Li and Zheng, 1993; Wang et al., 2019; Zhai et al., 2016), but there has been an absence of ophiolite mélange in a 700-km distance from central Tibet to southeastern Tibet. Our findings of the Bitu suture make this model admissible. Since the Longmu Co-Shuanghu suture, the Bitu suture, and the Changning-Menglian suture are all located along the north boundary of the eastern Cimmerian terrane, we infer that there is a connected Paleotethyan Ocean between the eastern Cimmerian and the Pamir-Qamdo micro-continents (Fig. 9a, Table 1).

We argue that the Bitu suture is a critical piece of the "jigsaw puzzle" in the Paleotethyan Ocean study in the Tibetan Plateau region, as it forms a complete suture system that bounded the eastern Cimmerian (Fig. 1a, Table 1). Based on this integrated suture zone, block correlation became possible for some orogenic belts in the Tibetan Plateau region. For example, the west Kunlun orogenic belt is divided into the Tarim, north Kunlun, south Kunlun, Tianshuihai, and Karakorum-South Pamir terranes from north to south (Fig. 10a). The South Qiangtang terrane is correlated with the Karakorum-South Pamir block, the Tianshuihai terrane with the North Qiangtang terrane, and the Songpan-Ganzi flysch belt with the South Kunlun terrane (e.g. Imrecke et al., 2019; Tang et al., 2020; Wang et al., 2020).

Before the establishment of the main Paleotethyan suture system, block correlations have been controversial between the Qiangtang terrane in central Tibet and those in southeastern Tibet (e.g. Metcalfe, 2006; Pan et al., 2012; Royden et al., 2008). While the Qiangtang is bounded by the Jinshajiang Paleotethyan suture to the north and the Bangong-Nujiang Mesotethyan suture to the south, the Simao terrane in southeastern Tibet is bounded by two Plaeotethyan sutures, the Jinshajiang to the east and the Changning-Menglian to the west. To the west, the Baoshan terrane is bounded by the Changning-Menglian Paleotethyan suture to the east and the Bangong-Nujiang Meso-Tethyan suture to its west. Additionally, the Simao terrane is featured with the Cathaysian affinity and the Baoshan terrane with Gondwana affinity. Based on this study, the South Qiangtang and the Baoshan terranes can be both classified as part of the eastern Cimmerian continent, and the North Qiangtang and Simao terranes are part of the Pamir-Qamdo continent (Fig.9a, Table 1). Southward, the Changning-Menglian suture can be correlated with the Inthanon suture, the Sukhothai granite belt with the Lincang volcanic belt, and the Khorat-Vientiane basin with the Simao-Qamdo basin (Fig. 10b) (e.g. Ueno, 2003; Sone and Metcalfe, 2008; Metcalfe, 2013; Wang et al., 2014: Li et al., 2019). Consequently, the Sibumasu terrane is the southern segment of the eastern Cimmerian continent, and the Indochina terrane is the southern segment of the Pamir-Qamdo continent (Fig.9a). The block correlation between Tibet and the vicinity reaffirmed the positions of the Cimmerian and Pamir-Qamdo ribbon-like micro-continents in the tectonic reconstruction of the Paleotethyan period (Fig. 9a).

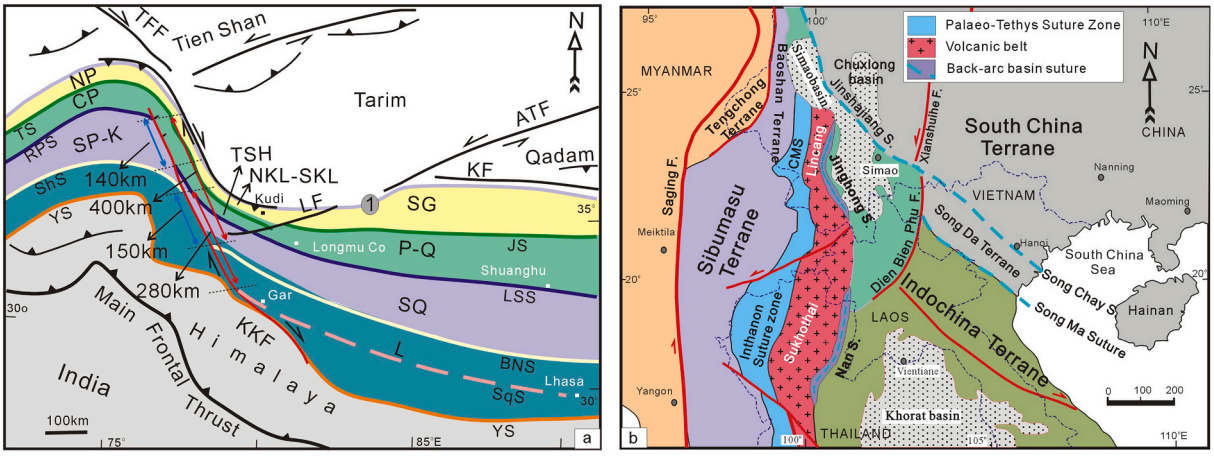

Fig. 10. (a) Preliminary correlation of tectonic blocks among the Pamir Plateau, the Tibetan Plateau, and Southeastern Asia (After Wang et al., 2020); (b) Blocks correlation from the Tibetan Plateau to Southeast Asia (After Metcalfe et al., 2013; Wang et al., 2016). Sutures/faults abbreviations: ATF: Altyn Tagh fault; BNS: Bangong-Nujiang suture; CMS: Changning-Menglian suture; JS: Jinshajiang suture; KF: East Kunlun fault; KKF-Karakoram fault; KS: Kudi suture; LF: Longmu Co fault; LSS: Longmu Co-Shuanghu suture; RPS: Rushan-Pshart suture; ShS: Shyok suture; SqS=Shiquanhe suture; TS: Tanymas suture; TTF: Talas-Fergana fault; YS: Yalong–Indus suture. Continental blocks: CP = Central Pamir; L = Lhasa; NKL-SKL: North Kunlun-South Kunlun; P-Q = Central Pamir-North Qiangtang-Qamdo-Indochina; S = Sibumasu; SG = Songpan-Ganzi; SP-K = South Pamir-Karakorum; SQ = South Qiangtang. TSH = Tianshuihai.

5.3. Deformation of the Tibetan plateau in the Cenozoic: Constraints from the main Paleotethyan suture system

The collision between India and Eurasia in the Cenozoic has largely shaped the present tectonics of the Tibetan Plateau (Yin and Harrison, 2000). Competing hypotheses exist to explain the deformation of the Tibetan Plateau, such as the crustal thickening model, the rigid block escape model, and the viscous flow model (e.g. England and Houseman, 1985; Leloup et al., 1995; Royden et al., 1997). One prerequisite to study the Cenozoic deformation is to delineate the pre-Cenozoic structures accurately (e.g., Yin and Harrison, 2000; Zhang et al., 2012; Zhang and Tang, 2009). In the rigid block escape model, the Karakorum-Jiali-Ailaoshan fault system is considered as a boundary fault that accommodates the southeastward escape of the Indochina block for about 500 km. The 500 km distance is acquired based on the offset of the Bangong-Nujiang suture from the Rushan-Pshart along the Karakoram fault (KKF), the Jinshajiang suture from the Dien Bien Phu suture along the Ailaoshan-Red River fault, as well as the Khorat basin from the Chuxiong Basin or Sichuan Basin (e.g. Lacassin et al., 2004; Leloup et al., 1995; Schwab et al., 2004) (Fig.10). However, kinematic and chronologic studies along the southern segment of the KKF show the fault accumulated 60–150 km offset since its initiation at 18–12 Ma (e.g. Murphy et al., 2000; Phillips et al., 2004; Wang et al., 2012). Moreover, recent studies show that the Rushan-Pshart suture is a Paleotethyan suture and the Bangong-Nujiang suture is a Mesotethyan suture (e.g. Angiolini et al., 2013; Chapman et al., 2018; Wang et al., 2020); i.e., they do not belong to the same suture. Similarly, the Dien Bien Phu suture is a Cenozoic fault and the Song Ma suture is the southeastern extension of the Jinshajiang suture (e.g. Faure et al., 2014; Metcalfe, 2013; Wang et al., 2016). We argue that the Cenozoic offset based on a Jinshajiang-Dien Bien Phu correlation is unreliable. Instead, we obtain an offset of about 140 ± 10 km based on the correlation of the Rushan-Pshart suture to the Longmu Co-Shuanghu suture and the Shyok suture to the Bangong-Nujiang suture, and we consider this a reliable estimate (Fig. 10a, Table 1). We further argue that the correlation between the Khorat basin and the Chuxiong Basin is also questionable because they are located in different blocks (Fig. 10b). The Pamir-Qamdo and Cimmerian continents are thinned significantly at the eastern Himalayan syntaxis (Figs. 1a, 10b). This suggests ductile deformation the terranes experienced (Penney and Copley, 2021). This study highlights the importance of building a robust correlation among the pre-Cenozoic sutures and terranes to better evaluate the competing mechanisms for the Cenozoic tectonics of the Tibetan Plateau region.

6. Conclusions

In this study, we report on the geochronology and geochemistry of the Bitu ophiolite mélange suite in eastern Tibet. The existence of the 265 Ma gabbro, 426–234 Ma basalts, serpentinites, and cherts indicate a Paleozoic-aged suite of ophiolite mélange. Carboniferous schist and phyllite are mainly derived from fine-grained segments of the Bouma sequence. We attributed these 426–234 Ma basalt/gabbro samples to be part of the Paleotethyan suture in eastern Tibet. Geochemical and Isotopic features prefer the basalt SLY06 samples originated from the OIB environment with a post-orogenic extensional continental environment. The SLY07 MORB-type basalts should be associated with the opening stage of the Paleotethyan Ocean. And the gabbro SLY08 samples are originated in an OIB environment.

The chronological and geochemical data of the mafic rocks in this paper indicate that there is an expanded Paleotethyan Ocean named Bitu Ocean from Late Silurian to Late Permian. It connected the Longmu Co-Shuanghu Ocean to the west and the Changning-Menglian Ocean to the east. These Paleotethyan oceans formed a complete ocean system that separated the Cimmerian from the Pamir-Qamdo continent. This sheds light on terrane correlation in different regions for the Paleo-Mesozoic evolution of the Tibetan Plateau region. Moreover, reconstruction of the Paleotethyan suture system offers new constraints on the Tibetan Plateau tectonics in the Cenozoic. It questions the proposal of ~400-km offset along the Karakoram fault based on the correlation of the Bangong-Nujiang suture with the Rushan-Pshart suture, also challenges the suggestion of 500-km offset along the Ailaoshan-Red River fault based on the correlation of the Jinshajiang suture with the Dien Bien Phu suture. Instead, we obtained 140 ± 10 km offset along the KKF based on the correlation of the Rushan-Pshart suture with the Longmu Co-Shuanghu suture, which shows a distributed deformation feature of the faults in the Tibetan Plateau.

Declaration of Competing Interest

None.

Acknowledgments

This study was jointly supported by the National Key R&D Program of China (2018YFC1505001) and the National Natural Science Foundation of China (Grant No. U2002211). We thank Li Zhengyou and Duan Lei for their assistance during fieldwork and Michael Murphy for revising the manuscript. We also thank two anonymous reviewers and Dr. G. Shellnutt (Co-Editor-in-Chief) provided thoughtful and constructive reviews of the manuscript. YL is supported by the Governor's University Research Initiative (GURI) Funds from the State of Texas and the University of Houston.

Appendix A. Supplementary data

Supplementary data to this article can be found online at https://doi.org/10.1016/j.lithos.2021.106520.

References

Andersen, T., 2002. Correction of common lead in U-Pb analyses that do not report 204Pb. Chem. Geol. 192, 59–79.
Angiolini, L., Zanchi, A., Zanchetta, S., Nicora, A., Vezzoli, G., 2013. The Cimmerian geopuzzle: new data from South Pamir. Terra Nova 25, 352–360.
Blichert-Toft, J., Albarede, F., 1997. The Lu–Hf geochemistry of chondrites and the evolution of the mantle-crust system. Earth Planet. Sci. Lett. 148, 243–258.
Boehnke, P., Watson, E.B., Trail, D., Harrison, T.M., Schmitt, A.K., 2013. Zircon saturation re-revisited. Chem. Geol. 351, 324–334.
Bureau of Geology and Mineral Resources of Xizang Province (BGMRX), 1993. Regional Geology of Xizang Province (in Chinese). Geological Publishing House, Beijing, pp. 1–220.
Carter, A., Roques, D., Bristow, C., Kinny, P., 2001. Understanding Mesozoic accretion in Southeast Asia: significance of Triassic thermotectonism (Indochina Orogeny) in Vietnam. Geology 29 (3), 211–214.
Chapman, J., Scoggin, S., Kapp, P., Carrapa, B., Ducea, M., Worthington, J., Oimahmadov, I., Gadoev, M., 2018. Mesozoic to Cenozoic magmatic history of the Pamir. Earth Planet. Sci. Lett. 482, 181–192.
Collins, A., Kröner, A., Fitzsimons, I., Razakamanana, T., 2003. Detrital footprint of the Mozambique Ocean: U/Pb SHRIMP and Pb evaporation zircon geochronology of metasedimentary gneisses in Eastern Madagascar. Tectonophysics 375, 77–99.
Corfu, F., Hanchar, J., Hoskin, P., Kinny, P., 2003. Atlas of zircon textures. Rev. Mineral. Geochem. 53, 469–500.
Cui, J., Bian, X., Wang, J., Yang, K., Zhu, H., Zhang, J., 2006. Discovery of an unconformity between the lower Silur ian and Middle Devonian in the Tianshuihu area, southern Kangxiwar, West Kunlun, China. Geological Bulletin of China 25 (12), 1437–1440 (In Chinese with English Abstract).
Dilek, Y., Furnes, H., 2011. Ophiolite genesis and global tectonics: Geochemical and tectonic fingerprinting of ancient oceanic lithosphere.Geological. Society of America Bulletin 123 (3–4), 387–411.
England, P., Houseman, G., 1985. Role of lithospheric strength heterogeneities in the tectonics of Tibet and neighbouring regions. Nature 315, 297–301.
Fan, J., Li, C., Wang, M., Xie, C., Xu, W., 2015. Features, provenance, and tectonic significance of Carboniferous–Permian glacial marine diamictites in the Southern Qiangtang–Baoshan block, Tibetan Plateau. Gondwana Res. 28 (4), 1530–1542.
Fan, J., Li, J., Xie, C., Liu, Y., Xu, J., Chen, J., 2017. Remnants of late Permian–Middle Triassic Ocean islands in northern Tibet: Implications for the late-stage evolution of the Paleo-Tethys Ocean. Gondwana Res. 44, 7–21.
Faure, M., Lepvrier, C., Nguyen, V., Vu, T., Lin, W., Chen, Z., 2014. The South China block-Indochina collision: where, when, and how? J. SE Asian Earth Sci. 79, 260–274.

Feng, Q.L., Shen, S.Y., Liu, B.P., Helmcke, D., Qian, X.G., Zhang, W.M., 2002. Permian radiolarians, chert and basalt from the Daxinshan Formation in Lancangjiang belt of southwestern Yunnan, China. Science in China. Ser. D Earth Science 45 (1), 63–71.
Griffin, W.L., Pearson, N.J., Belousova, E., Jackson, S.E., van Achterbergh, E., O'Reilly, S. Y., Shee, S.R., 2000. The Hf isotope composition of cratonic mantle: LA–MC–ICP–MS analysis of zircon megacrysts in kimberlites. Geochim. Cosmochim. Acta 64, 133–147.
He, S.P., Li, R.S., Wang, C., Zhang, H.F., Ji, W.H., Yu, P.S., Gu, P.Y., Shi, C., 2011. Discovery of ~4.0 Ga detrital zircons in the Changdu Block, North Qiangtang, Tibetan Plateau. Chin. Sci. Bull. 56, 573–582.
Hoskin, P.W.O., Schaltegger, U., 2003. The composition of zircon and igneous and metamorphic petrogenesis. Rev. Mineral. Geochem. 53 (1), 27–62.
Hou, K.J., Li, Y.H., Zou, T.R., Qu, X.M., Shi, Y.R., Xie, G.Q., 2007. Laser ablation-MC-ICP-MS technique for Hf isotope microanalysis of zircon and its geological applications. Acta Petrol. Sin. 23, 2595–2604 (in Chinese with English abstract).
Imrecke, D.B., Robinson, A.C., Owen, L.A., Chen, J., Schoenbohm, L.M., Hedrick, K.A., Lapen, T.J., Li, W., Yuan, Z., 2019. Mesozoic evolution of the eastern Pamir. Lithosphere 11 (4), 560–580.
Irvine, T.N., Baragar, W.R.A., 1971. Guide to chemical classification of common volcanic rocks. Can. J. Earth Sci. 8 (5), 523–548.
Jian, P., Liu, D.Y., Sun, X.M., 2008. SHRIMP dating of the Permo-Carboniferous Jinshajiang ophiolite, southwestern China: geochronological constraints for the evolution of Paleo-Tethys. J. Asian Earth Sci. 32, 371–384.
Jian, P., Liu, D., Kroner, A., Zhang, Q., Wang, Y., Sun, X., Zhang, W., 2009a. Devonian to Permian plate tectonic cycle of the paleo-Tethys Orogen in Southwest China (I): geochemistry of ophiolites, arc/back-arc assemblages and within-plate igneous rocks. Lithos 113, 748–766.
Jian, P., Liu, D., Kröner, A., Zhang, Q., Wang, Y., Sun, X., Zhang, W., 2009b. Devonian to Permian plate tectonic cycle of the Paleo-Tethys Orogen in Southwest China (II): insights from zircon ages of ophiolites, arc/back-arc assemblages and within-plate igneous rocks and generation of the Emeishan CFB province. Lithos 113, 767–784.
Kapp, P., Yin, A., Manning, C.E., Murphy, M., Harrison, T.M., Spurlin, M., Ding, L., Deng, X.G., Wu, C.M., 2000. Blueschist-bearing metamorphic core complexes in the Qiangtang block reveal deep crustal structure of northern Tibet. Geology 28, 19–22.
Lacassin, R., Valli, F., Arnaud, N., Leloup, P.H., Paquette, J.L., Li, H., Tapponnier, P., Chevalier, M.L., Guillot, S., Maheo, G., Xu, Z., 2004. Large-scale geometry, offset and kinematic evolution of the Karakoram fault, Tibet. Earth and Planet Science Letter 219 (3–4), 255–269.
Leloup, P.H., Lacassin, R., Tapponnier, R., Zhong, D., Lui, X., Zhang, L., Ji, S., Trinh, P.T., 1995. The Ailao Shan–Red River shear zone (Yunnan, China), Tertiary transform boundary of Indochina. Tectonophysics 251, 3–84.
Li, C., Zheng, A., 1993. Paleozoic stratigraphy in the Qiangtang region of Tibet: Relations of the Gondwana and Yangtze continents and ocean closure near the end of the Carboniferous. Int. Geol. Rev. 35 (9), 797–804.
Li, C., Huang, X., Zhai, Q., 2006. The Longmu Co-Shuanghu-Jitang plate suture and the northern boundary of Gondwanaland in the Qinghai-Tibet plateau. Earth Science Frontiers 13 (4), 136–147 (In Chinese with English Abstract).
Li, C., Xie, Y.W., Dong, Y.S., Xu, F., Qiangba, Z.X., Jiang, G.W., 2009. The north Lancangjiang suture: the boundary between Gondwana and Yangtze? Geological Bulletin of China 28 (12), 1711–1719 (In Chinese with English abstract).
Li, S., Zhao, S., Liu, X., Cao, H., Yu, S., Li, X., Somerville, I., Yu, S., Suo, Y., 2018. Closure of the Proto-Tethys Ocean and early Paleozoic amalgamation of microcontinental blocks in East Asia. Earth Sci. Rev. 186, 37–75.
Li, S., Chung, S.L., Hou, Z., Chew, D., Wang, T., Wang, B., Wang, Y., 2019. Early Mesozoic magmatism within the Tibetan Plateau: Implications for the Paleo-Tethyan tectonic evolution and continental amalgamation. Tectonics 38, 3505–3543.
Liu, Y., Hu, Z.C., Gao, S., Günther, D., Xu, J., Gao, C.G., Chen, H.H., 2008. In situ analysis of major and trace elements of anhydrous minerals by LA–ICP–MS without applying an internal standard. Chem. Geol. 257, 34–43.
Ludwig, K.R., 2003. Users Manual for Isoplot/Ex rev. 3.0, Spec. Publ. 1a, Berkeley Geochronol. Cent., Berkeley, Calif.
Meschede, M., 1986. A method of discriminating between different types of mid-ocean ridge basalts and continental tholeiites with the Nb-Zr-Y diagram. Chem. Geol. 56 (3–4), 207–218.
Metcalfe, I., 2006. Palaeozoic and Mesozoic tectonic evolution and palaeogeography of East Asian crustal fragments: the Korean Peninsula in context. Gondwana Res. 9, 24–46.
Metcalfe, I., 2013. Gondwana dispersion and Asian accretion: tectonic and palaeogeographic evolution of the eastern Tethys. J. Asian Earth Sci. 66, 1–33.
Middlemost, E.A.K., 1994. Naming materials in the magma/igneous rock system. Earth-Sci. Rev. 37, 215–224.
Murphy, M.A., Yin, A., Kapp, P., Harrison, T.M., Lin, D., Jinghui, G., 2000. Southward propagation of the Karakoram fault system, Southwest Tibet: timing and magnitude of slip. Geology 28 (5), 451–454.
Niu, Y., 2009. Some basic concepts and problems on the petrogenesis of intra-plate ocean island basalts. Chin. Sci. Bull. 54, 4148–4160.
Pan, G., Wang, L., Li, R., Yin, F., Zhu, D., 2012. Tectonic model of archipelagic arc-basin systems: the key to the continental geology. Sedimentary Geology and Tethyan Geology 32 (3), 516 (in Chinese with English abstract).
Pearce, J.A., 1982. Trace element characteristics of lavas from destructive plate boundaries. In: Thorpe, R.S. (Ed.), Andesites: Orogenic Andesites and Related Rocks. Willy, Chichester, pp. 525–548.
Pearce, J.A., 2008. Geochemical fingerprinting of oceanic basalts with applications to ophiolite classification and the search for Archean oceanic crust. Lithos 100 (1–4), 14–48.
Peng, T., Zhao, G., Fan, W., Peng, B., Mao, Y., 2015. Late Triassic granitic magmatism in the eastern Qiangtang, eastern Tibetan Plateau: Geochronology, petrogenesis and implications for the tectonic evolution of the Paleo-Tethys. Gondwana Res. 27 (4), 1494–1508.
Penney, C., Copley, A., 2021. Lateral variations in lower crustal strength control the temporal evolution of mountain ranges: examples from south-east Tibet. Geochemistry, Geophysics, Geosystems 22 (2) (p.e2020GC009092).
Phillips, R.J., Parrish, R.R., Searle, M.P., 2004. Age constraints on ductile deformation and long-term slip rates along the Karakorum fault zone, Ladakh. Earth Planet. Sci. Lett. 226, 305–319.
Pullen, A., Kapp, P., Gehrels, G.E., Vervoort, J.D., Ding, L., 2008. Triassic continental subduction in Central Tibet and Mediterranean-style closure of the Paleo-Tethys Ocean. Geology 36 (5), 351–354.
Robinson, A., 2015. Mesozoic tectonics of the Gondwanan terranes of the Pamir plateau. J. Asian Earth Sci. 102, 170–179.
Rollinson, H.R., 1993. Using Geochemical Data: Evaluation, Presentation, Interpretation. John Wiley & Sons, New York, p. 155.
Royden, L.H., Burchfi el, B.C., King, R.W., Chen, Z., Shen, F., Liu, Y., 1997. Surface deformation and lower crustal fl ow in eastern Tibet: Science, 276, 788–790. https://doi.org/10.1126/science.276.5313.788.
Royden, H.L., Burchfiel, B.C., van der Hilst, D.R., 2008. The Geological Evolution of the Tibetan Plateau. Science 321, 1054–1058.
Schwab, M., Ratschbacher, L., Siebel, W., McWilliams, M., Minaev, V., Lutkov, V., Chen, F., Stanek, K., Nelson, B., Frisch, W., Wooden, J.L., 2004. Assembly of the Pamirs: Age and origin of magmatic belts from the southern Tien Shan to the southern Pamirs and their relation to Tibet. Tectonics 23, TC4002.
Sengor, A.M.C., 1979. Mid-Mesozoic closure of Permo-Triassic Tethys and its implications. Nature 279, 590–593.
Shervais, J.W., 1982. Ti-V plots and the petrogenesis of modern and ophiolitic lavas. Earth Planet. Sci. Lett. 59 (1), 101–118.
Sone, M., Metcalfe, I., 2008. Parallel Tethyan suture in mainland Southeast Asia: New insights from Paleo-Tethys closure and implications for the Indosinian orogeny. Compt. Rendus Geosci. 340, 166–179.
Stampfli, G.M., Hochard, C., Vérard, C., Wilhem, C., von Raumer, J., 2013. The formation of Pangea. Tectonophysics 593, 1–19.
Sun, S.S., McDonough, W.F., 1989. Chemical and Isotopic Systematics of Oceanic Basalts: Implications for Mantle Composition and Processes. In: Saunders, A.D., Norry, M.J. (Eds.), Magmatism in the Ocean Basins, Geological Society, London, Special Publications, vol. 42, pp. 313–345.
Tang, X.C., Zhang, K.J., 2014. Lawsonite- and glaucophane-bearing blueschists from NW Qiangtang (northern Tibet, China): Mineralogy, geochemistry, geochronology, and tectonic implications. Int. Geol. Rev. 56, 150–166.
Tang, W., Wang, S., Liu, Y., Yao, X., Li, M., 2020. Origin of Carboniferous intra-oceanic arc granitoids from the eastern Pamir and implication on the Paleo-Tethyan ocean. J. Asia Earth Sci. 204, 104558.
Tao, Y., Bi, X., Li, C., Hu, R., Li, Y., Liao, M., 2014. Geochronology, petrogenesis and tectonic significance of the Jitang granitic pluton in eastern Tibet, SW China. Lithos 184-187, 314–323.
Ueno, K., 2003. The Permian fusulinoidean faunas of the Sibumasu and Baoshan blocks: their implications for the paleogeographic and paleoclimatologic reconstruction of the Cimmerian Continent. Palaeogeogr. Palaeoclimatol. Palaeoecol. 193, 1–24.
Wang, S., Wang, C., Phillips, R.J., Murphy, M.A., Fang, X., Yue, Y., 2012. Displacement along the Karakoram fault, NW Himalaya, estimated from LA-ICP-MS U–Pb dating of offset geologic markers. Earth Planet. Sci. Lett. 337, 156–163.
Wang, B., Wang, L., Pan, G., 2013. U-Pb zircon dating of early Paleozoic gabbro from the Nantinghe ophiolite in the Changning-Menglian suture zone and its geological implication. Chin. Sci. Bull. 58, 344–354.
Wang, L., Liu, C., Gao, X., Zhang, H., 2014. Provenance and paleogeography of the late cretaceous Mengyejing Formation, Simao Basin, southeastern Tibetan Plateau: Whole-rock geochemistry, U-Pb geochronology, and Hf isotopic constraints. Sediment. Geol. 304, 44–58.
Wang, M., Li, C., Xie, C., Xu, J., Li, X., 2015. U–Pb zircon age, geochemical and Lu–Hf isotopic constraints of the Southern Gangma Co basalts in the Central Qiangtang, northern Tibet. Tectonophysics 657, 219–229.
Wang, S., Mo, Y., Wang, C., Ye, P., 2016. Paleotethyan evolution of the Indochina block as deduced from granites in northern Laos. Gondwana Res. 38, 183–196.
Wang, S., Yao, X., Jiang, W., 2019. Geochronological, geochemical, and Sr–Nd–Hf isotopic characteristics of granitoids in eastern Tibet and implications for tectonic correlation with southeastern Asia. Lithosphere 11 (3), 333–347.
Wang, S., Tang, W., Liu, Y., Yao, X., 2020. Rushan-Pshart Paleo-Tethyan suture deduced from geochronological, geochemical, and Sr-Nd-Hf isotopic characteristics of granitoids in Pamir. Lithos 364-365, 105549.
Wu, G., 2006. Bitu ophiolite in the Zuogong area, eastern Tibet: Geological records of Paleo-Tethyan major oceanic basin. Geological Bulletin of China 25 (6), 685–693.
Wu, H., Boulter, C.A., Ke, B., Stow, D.A.V., Wang, Z., 1995. The Changning-Menglian suture zone; a segment of the major Cathaysian -Gondwana divide in Southeast Asia. Tectonophysics 242, 267–280.
Xia, J., Zhong, H., Tong, J., Lu, R., 2006. Unconformity between the lower Ordovician and Devonian in the Sanchakou area in the easter part of the Longmu Co, northern Tibet, China. Geological Bulletin of China 25 (1–2), 113–117 (In Chinese with English Abstract).
Xiao, W., Huang, B., Han, C., Sun, S., Li, J., 2010. A review of the western part of the Altaids: a key to understanding the architecture of accretionary orogens. Gondwana Res. 18, 253–273.
Yin, A., Harrison, T.M., 2000. Geologic Evolution of the Himalayan-Tibetan Orogen. Annu. Rev. Earth Planet. Sci. 28, 211–280.

Zhai, Q., Jahn, B., Wang, J., Hu, P., Chung, S., Lee, H., Tang, S., 2016. Oldest Paleo-Tethyan ophiolitic mélange in the Tibetan Plateau. Geology Society of American Bulletin 128 (3/4), 355–373.

Zhang, K.J., 2001. Blueschist-bearing metamorphic core complexes in the Qiangtang block reveal deep crustal structure of northern Tibet: comment. Geology 29, 90.

Zhang, K.J., Tang, X.C., 2009. Eclogites in the interior of the Tibetan plateau and their geodynamic implications. Chin. Sci. Bull. 54, 2556–2567.

Zhang, K.J., Zhang, Y.X., Li, B., Zhu, Y.T., Wei, R.Z., 2006a. The blueschist-bearing qiangtang metamorphic belt (northern Tibet, China) as an in situ suture zone: evidence from geochemical comparison with the Jinsa suture. Geology 34 (6), 493–496.

Zhang, K.J., Cai, J.X., Zhang, Y.X., Zhao, T.P., 2006b. Eclogites from central Qiangtang, northern Tibet (China) and tectonic implications. Earth Planet. Sci. Lett. 245, 722–729.

Zhang, K.J., Zhang, Y.X., Tang, X.C., Xia, B., 2012. Late Mesozoic tectonic evolution and growth of the Tibetan plateau prior to the Indo–Asian collision. Earth Sci. Rev. 114, 236–249.

Zhang, Y.C., Shi, G.R., Shen, S.Z., 2013. A review of Permian stratigraphy, palaeobiogeography and palaeogeography of the Qinghai-Tibet Plateau. Gondwana Res. 24 (1), 55–76.

Zhang, Y.X., Jin, X., Zhang, K.J., Sun, W.D., Zhou, X.Y., Yan, L.L., 2018. Newly discovered late Triassic Baqing eclogite in Central Tibet indicates an anticlockwise West–East Qiangtang collision. Scientific Report 8 (966). https://doi.org/10.1038/s41598-018-19342-w.